# Characterizing the Microwave Properties of Multi-Qubit cQED Devices with Purcell Filter for Multiplexed Readout

Toni Heugel
*Semester Thesis, Department of Physics, ETH Zürich*
*Supervisors: Yves Salathé and Prof. Dr. Andreas Wallraff*

June 22, 2016

**Abstract**

In this semester thesis the microwave properties of single resonators and systems of coupled resonators are investigated. The resonance frequencies, the quality factors, the internal and external quality factor and the insertion loss at 4.2 K and at 20 mK are determined using measurements and simulations. Two designs with multiplexed readout are analysed and the coupling strength of the readout resonators is determined. The dependence of the quality factor on the number of photons is investigated and an effective permittivity for the mask is extracted from measurements at 20 mK. Additionally the crosstalk of a chip with resonators for multiplexed readout and for nearest-neighbour coupling, charge lines and flux bias lines is analysed.

## Contents

# 1 Introduction

Moore's law "The number of transistors on a piece of silicon doubles every couple of years." (Gordan E. Moore 1965) is valid for more than the last 40 years. But in the future the transistors would be so small, that quantum mechanical effects like the tunnelling current occur. This might be a crucial problem for shrinking transistors. One idea is to start a new approach and work with qubits which can not be only in the state zero or one but also in a superposition of them. Using a quantum computer based on such qubits, quantum systems could be simulated more effectively and certain types of problems could be solved within shorter time. Here the approach is to use superconducting circuits as qubits. The main focus of the project so far is to build a basic module which can be symmetrically copied to obtain a system with more qubits. This basic element consists of four qubits, whereby nearest-neighbour qubit-qubit coupling is achieved by coupling resonators. Unwanted coupling is expected to be suppressed by the spacing between the qubits and by choosing different frequencies for the resonator. Multiplexed readout of four qubits is provided by individual readout resonators coupled to the Purcell filter[2].

In this semester thesis the microwave properties of the resonators used for qubit-qubit coupling and multiplexed readout are characterized and analysed. The chips are produced using lithography techniques and tested in liquid helium (4.2 K) as well as in a dilution cryostat at base temperature (20 mK). A vector network analyser is used to measure the transmission spectra from which the quality factor $Q$ is determined as well as the resonance frequency $f_0$ and the insertion loss $L_0$ of the resonator. This will be done for several resonators of different length and different coupling capacities. One goal is to find a configuration of a Purcell filter and four readout resonators such that two resonances of the readout resonators are located below and two above the resonance frequency of the Purcell filter. At the same time these resonances should be close to the Purcell filter peak but one should be able to distinguish between all resonances. This is an important ingredient to perform multiplexed readout of the qubit states. The software AWR Design Environment is used to simulate the transmission spectra of the resonators. This is used to determine the external quality factor $Q_e$ and the resonance frequency $f_0$, which are compared with the measurements. Using the measured and simulated data, the internal quality factor $Q_i$ and the insertion loss $L_0$ can be calculated.

During the measurements in the dilution cryostat the input power at the resonator was swept in addition to the frequency to investigate the dependency of $Q$ on the estimated number of photons in the resonator in a range of several to millions of photons. This is important to know, since the qubit readout is performed with about one photon in the Purcell filter.

A further goal is to analyse the crosstalk between the charge and flux lines to the Purcell filter. It is crucial that the measurement of the states is not affected and disturbed. So the crosstalk should be minimized.

| | | | |
|---|---|---|---|
| $l_{C6}$ in µm | 7790 | $C_{in}$ in fF | 25 |
| $l_{B2}$ in µm | 6926 | $C_{out}$ in fF | 120 |
| $l_{RR1}$ in µm | 4310.3 | $C_{toPF}$ in fF | 18 |
| $l_{RR2}$in µm | 4260.3 | $C_{toGrnd}$ in fF | 73 |
| $l_{RR3}$ in µm | 4212.3 | | |
| $l_{RR4}$ in µm | 4164.3 | | |

Table 1: Length of the Purcell filter on chip M57C6 $l_{C6}$ and on M57B2 $l_{B2}$, length of the readout resonators $l_{RR1}$, $l_{RR3}$, $l_{RR2}$ and $l_{RR4}$ (from left to right). Coupling capacitance at the input $C_{in}$ and output $C_{out}$, capacitance form the readout resonator to Purcell filter $C_{toPF}$ and to ground $C_{toGrnd}$.

In the following, the samples are presented and their properties are given. Chapter three shows the used measurement methods in liquid helium and in the dilution cryostat. Thereafter the measurements results are presented, discussed and compared to the simulations. In the last chapter the conclusions are drawn and improvements are proposed.

## 2 Samples

The samples which were characterized in this thesis are presented and discussed in this section. Basically three types of resonators were analysed. The first is a single under-coupled Purcell filter which was investigated for different resonance frequencies and coupling capacities. Further we looked at the coupling resonators connected to two qubit holders with different resonance frequencies. The last type is a system of resonators consisting of one Purcell filter which is coupled to four readout resonators as can be seen in Figure 1.
The chips are made using standard optical lithography techniques.

On M57C6 and M57B2 there are a Purcell filter and four readout resonators which can be coupled to qubits in later experiments. The conceptual design is shown in Figure 1. The Purcell filter is used for multiplexed readout allowing fast measurements, whereby environmental damping of the qubit is suppressed [2]. The Purcell filter is a $\lambda/2$ resonator, whereas the readout resonators are $\lambda/4$ resonators. The qubits are also provided with flux bias and charge lines. The lengths and capacitances of the used resonators are presented in Table 1.

The Purcell filters and the coupling resonators were analysed on the chips M57A3, M57A4, M57B1 and M57F3. The circuits are depicted in Figure 2. The Purcell filters are connected to the measuring instruments by wire bonds at the input (left side) and the output (right side). Coupling capacitors transmit the incoming signals to the Purcell filter consisting of a coplanar wave guide line. The curves in the middle extend the resonators

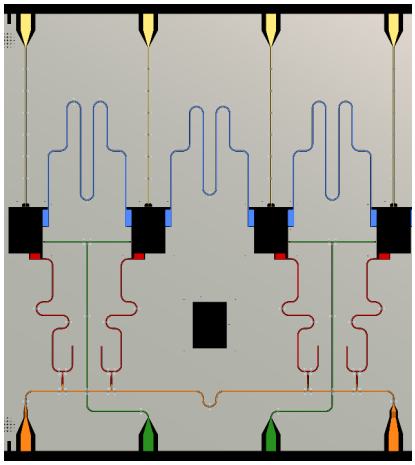

Figure 1: Design of M57C6 and M57B2: The four black boxes in a line are gaps for qubits in later experiments. They are connected by coupling resonators (blue). Every qubit has its own flux bias line (yellow) and pairs of qubits are coupled to charge lines (green). For the readout of the qubit states one uses resonators (red) coupled to a Purcell filter (orange).

to lower the resonance frequency which is given by [1]

$$f_0 = \frac{c}{2l\sqrt{\epsilon_{eff}}}. \tag{1}$$

Here, $c$ is the speed of light in vacuum, $l$ is the length of the resonator and $\epsilon_{eff}$ the effective permittivity of the coplanar wave guide. $\epsilon_{eff}$ depends on the wave guide geometry and the relative permittivities of the substrate and the oxide layer. By changing the length $l$ of the resonator one can change its resonance frequency while the coupling capacitors affect the quality factor $Q$ of the resonator. The length $l$ and the coupling capacitances $C_{in}$ and $C_{out}$ of the Purcell filters are shown in Table 2. The given lengths do not include the additional effective length of the finger capacitor (80 µm) and the T-junctions. The Purcell filter on M57A4 is coupled by finger capacitors while on M57A3, M57B1 and M57F3 the connection is made by 30 µm gap capacitors. M57A3 is extended by T-junctions whereby this chip differs from M57B1. Furthermore, M57B1 contains charge lines.

The coupling resonators are the same on all chips. At the left side the resonator is designed to be at 8 GHz and at the right side to be at 8.5 GHz. They are shown in Figure 2. Input and output coplanar waveguides are connected to qubit gaps such that they couple to the coupling resonators. The length $l$ of the resonators and the coupling resonators can be seen in Table 3. The pad at both ends of the resonator has a capacitance to the input/ output line as well as to the ground plane. The given capacitances were simulated using Ansys Maxwell.

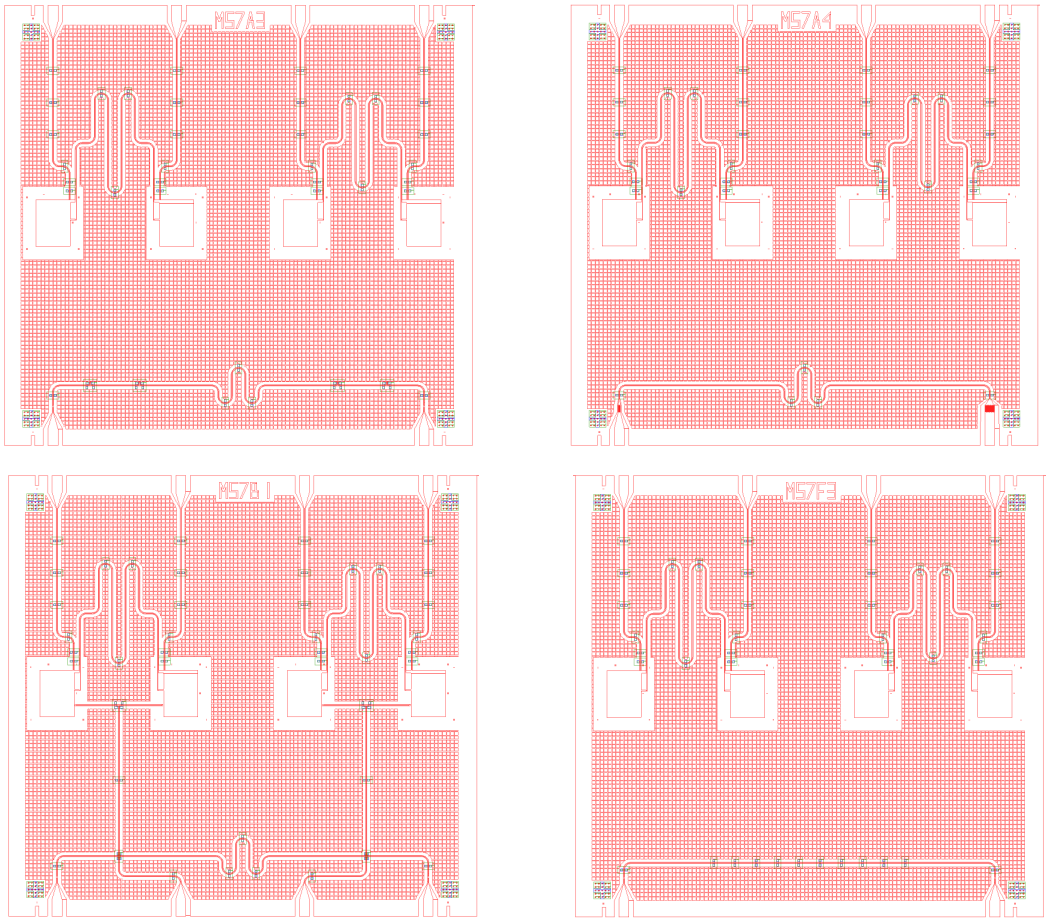


Figure 2: Illustration of the chips M57A3, M57A4, M57B1 and M57F3. The upper resonators on the chips are the coupling resonators (left one at 8 GHz, right one at 8.5 GHz) and the lower the under-coupled equivalents to the Purcell filters.

| Purcell filter | $l$ in µm | $C_{in}$ in fF | $C_{out}$ in fF |
|---|---|---|---|
| M57A3 | 7306 | 0.32 | 0.32 |
| M57A4 | 7386 | 25 | 120 |
| M57B1 | 7306 | 0.32 | 0.32 |
| M57F3 | 5884 | 0.32 | 0.32 |

Table 2: Length $l$, coupling capacitance at the input $C_{in}$ and at the output $C_{out}$ of the Purcell filters.

| Coupling resonator | $l$ in µm | Capacitance resonator to the in/output line in fF | Capacitance resonator to ground plane in fF |
|---|---|---|---|
| at 8 GHz | 7500 | 1.5 | 64.5 |
| at 8.5 GHz | 7000 | 1.5 | 64.5 |

Table 3: Length $l$ and capacitances of the coupling resonators.

# 3 Measurements Methods

In this experiment we measured the scattering-parameters (s-parameter) of the different resonators on the chips as well as the crosstalk between the ports at 4.2 K and determined the resonance frequency $f_0$ and the quality factor $Q$. The sample was mounted onto a sample holder (dipstick) and inserted in a dewar filled with liquid helium. The measurements were performed by the vector network analyser N5230C (VNA) from Keysight which was calibrated using the Rosenberger SMP calibration kit model 19CK 10A-150.

The dipstick consists of SMA connectors on the top which are connected to SMP connectors at the bottom by stainless steel cables. The dipstick is cooled down to 4.2 K and heated up to room temperature whereby the cables are deformed. To relieve the tension onto the connectors the cables have bends. A further advantage is the extension of the cables which lowers the heat gradient and hence the heat transfer to the sample. The sample holder is located at the bottom and made of copper.

To perform these measurements a VNA is used to send an AC signal with a certain power to an input port and measure the reflected as well as the transmitted complex amplitude of the signal. The signal frequency is swept and the measurements are repeated and averaged. The input power, number of points of the frequency sweep, number of averages and IF bandwidth was adapted for the different measurements. For the calibration of the VNA (measurement at 4.2 K) we used a Rosenberger calibration kit consisting of an open, a short, a load and a through plug. In this experiment the cables from the VNA to the dipstick as well as the cables in the dipstick and the connectors at the sample holder were calibrated. The measurements of the chips M57A4, M57B2 and M57F3 could not be calibrated with th Rosenberger kit since here another VNA without calibration data was used. However, we measured the transmission of a through plug at 4.2 K and corrected the

measurements on the chips M57A4, M57B2 and M57F3.

In addition to the measurement in liquid helium the measurements of the chips M57A3 and M57B1 were also performed at a base temperature of 20 mK in a dilution cryostat. In the process the input power was swept (from around 10 up to several millions of photons). In the dilution cryostat we measured without calibration of the probe cables.

# 4 Results and Discussion

The measured complex transmission amplitude of the resonators was fitted by a complex Lorentzian as discussed later. This allowed us to determine the resonance frequency $f_0$ and the quality factor $Q$ of the resonators.

First an overview of these results is given and afterwards the raw data and the fits are presented. The fitting methods and the fit parameters are explained and discussed. The quality factor $Q$ of the resonator depending on the number of photons in the resonator was determined with power sweep measurements in the dilution cryostat. The measurements are compared with the simulations made by AWR Design Environment (AWR). Thereafter the internal quality factor $Q_{int}$ and the insertion loss $L_0$ are calculated using the expected external quality factor from the simulations below. At last the crosstalk is shown and analysed.

The resonance frequency of the Purcell filter $f_0$ and of the readout resonators $f_1$, $f_2$, $f_3$ and $f_4$ and the quality factor of the Purcell filter $Q$ of the chips M57C6 and M57B2 are presented in Table 4. The resonance frequency $f_0$ and the quality factor of the single resonators on the chips M57A3, M57A4, M57B1 and M57F3 are presented in Table 5.

| at 4.2 K | M57C6 | M57B2 |
|---|---|---|
| $f_0$ in GHz | $6.5629 \pm 0.0002$ | $7.3126 \pm 0.0004$ |
| $f_1$ in GHz | $7.00847 \pm 0.00002$ | $7.0144 \pm 0.0001$ |
| $f_2$ in GHz | $7.09695 \pm 0.00002$ | $7.10121 \pm 0.00008$ |
| $f_3$ in GHz | $7.1684 \pm 0.0001$ | $7.17527 \pm 0.00004$ |
| $f_4$ in GHz | $7.25358 \pm 0.00005$ | $7.25808 \pm 0.00007$ |
| $Q$ | $31.15 \pm 0.05$ | $20.84 \pm 0.04$ |

Table 4: Measured resonance frequencies of the Purcell filter $f_0$ and the readout resonators $f_1$, $f_2$, $f_3$ and the measured quality factor $Q$ of the chips M57C6 and M57B2.

**Discussion of Fitting and Results:**

**Measurements at 4.2 K:** To determine the quality factor and the resonance frequency the measured transmission data was fitted as explained below. In Figure 3 and 4

| | $f_0$ in GHz | $Q$ |
|---|---|---|
| PF M57A3 at 4.2 K | $8.27127 \pm 0.00001$ | $809 \pm 2$ |
| PF M57A3 at 20 mK | $8.3102138 \pm 7 \times 10^{-}7$ | $253000 \pm 6000$ |
| PF M57A4 at 4.2 K | $7.5706 \pm 0.0001$ | $21.35 \pm 0.01$ |
| PF M57B1 at 4.2 K | $8.49792 \pm 0.00007$ | $1113 \pm 22$ |
| PF M57B1 at 20 mK | $8.5132131 \pm 7 \times 10^{-}7$ | $145000 \pm 1000$ |
| PF M57F3 at 4.2 K | $10.5810 \pm 0.0001$ | $358 \pm 3$ |
| CR at 8 GHz at 4.2 K | $8.0041 \pm 0.0029$ | $1433 \pm 128$ |
| CR at 8 GHz at 20 mK | $8.031852 \pm 2 \times 10^{-}6$ | $102500 \pm 300$ |
| CR at 8.5 GHz at 4.2 K | $8.5153 \pm 0.0078$ | $1456 \pm 87$ |

Table 5: Measured resonance frequency $f_0$ as well as the measured quality factor $Q$ of the Purcell filter (PF) and the coupling resonators (CR) on the chips M57A3, M57A4, M57B1 and M57B2. The values of the coupling resonators are the averages of the measurements. The measurements in liquid helium (4.2 K) are performed at an input power (at the resonator) of approximately - 93 dBm and the measurements in the dilution cryostat (20 mK) at -94 dBm. This is the power of the signal produced by the VNA attenuated by about 85 dBm from the cables and attenuators.

the transmission data and the fit of the chips M57C6 and M57B2 are shown. The data and the fits of the Purcell Filter and the coupling resonators on the chips M57A3, M57A4, M57B1 and M57F3 are presented in Table 6. In the following, the fitting methods and fitting parameters are discussed.

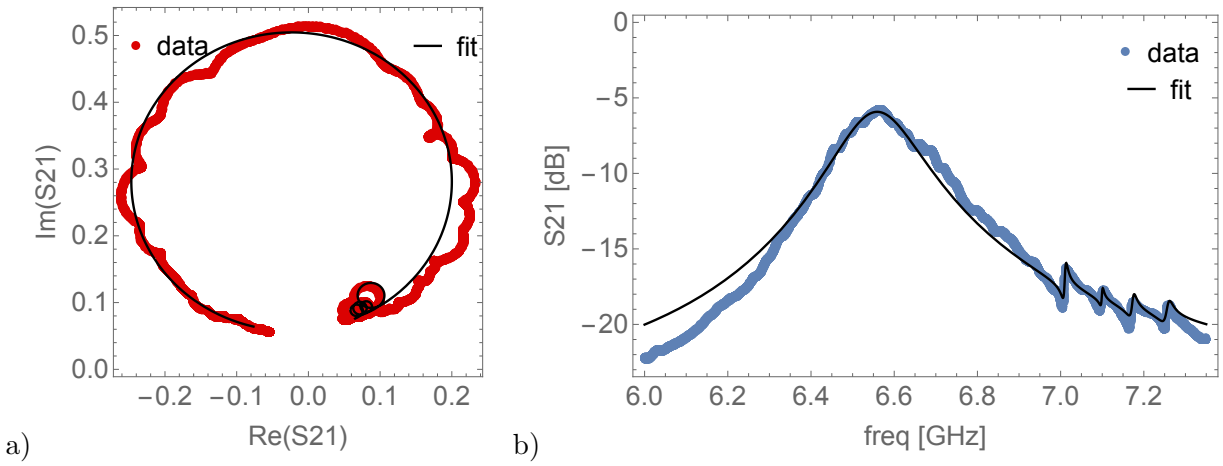


Figure 3: Measured data of chip M57C6 at 4.2 K: a) Polar plot of the measured complex transmission amplitude S(2,1) and a fit using the input/output model described in the main text. b) Transmission coefficient through the Purcell filter in dB depending on the frequency and the same fit function as in a).

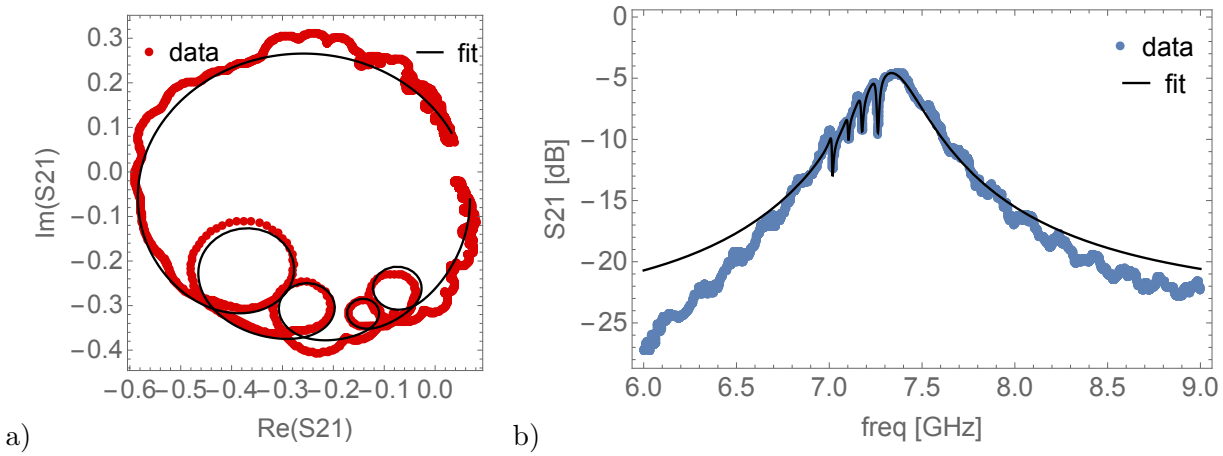


Figure 4: Measured data of chip M57B2 at 4.2 K: a) Polar plot of the measured complex transmission amplitude S(2,1) and a fit using the input/output model described in the main text. b) Transmission coefficient through the Purcell filter in dB depending on the frequency and the same fit function as in a).

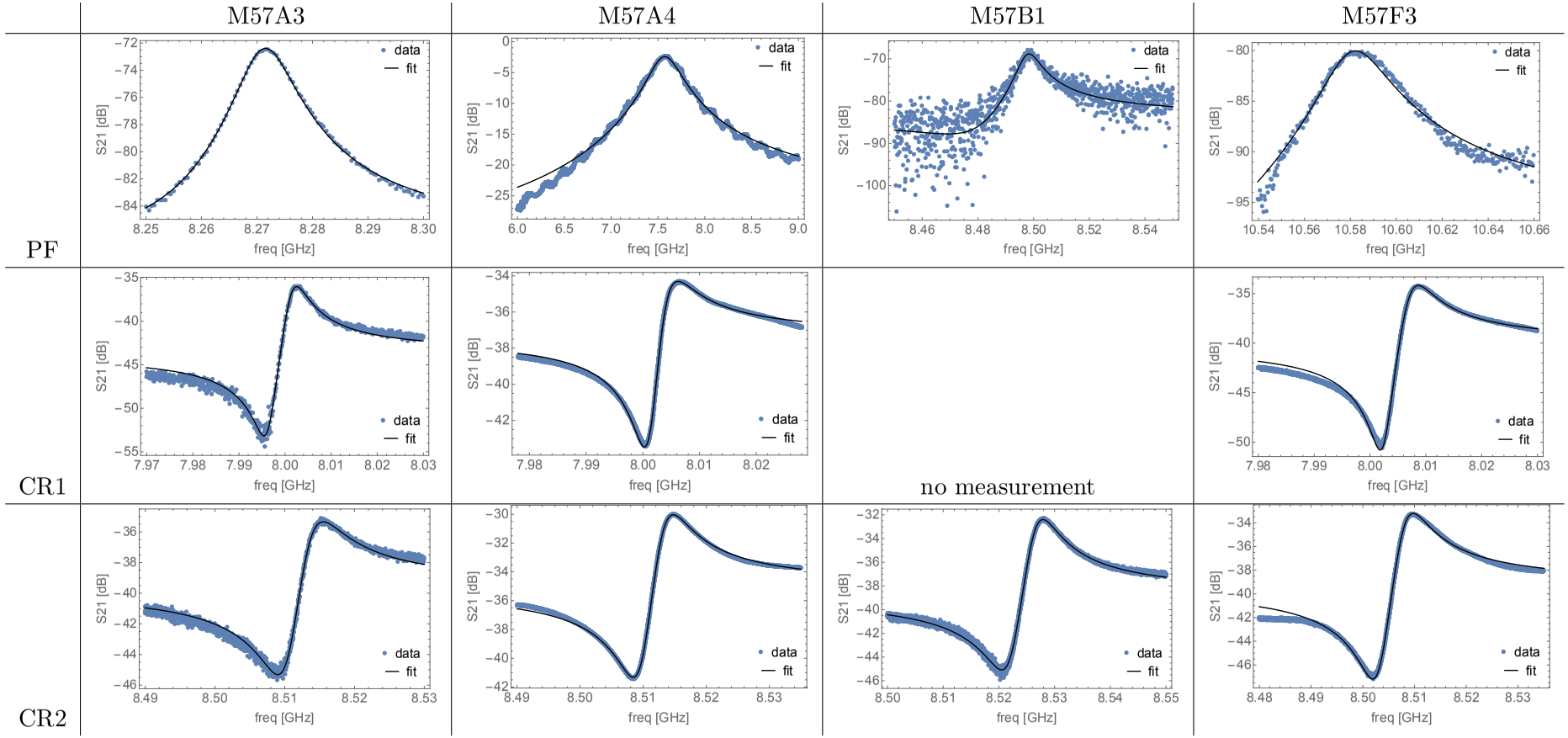


Table 6: Transmission coefficient through the Purcell filter(PF), the coupling resonator at 8 GHz(CR1) and the the coupling resonator at 8.5 GHz(CR2) depending on the frequency measured at 4.2 K and a complex Lorentzian fit.

The measured complex amplitude S(2,1) depending on the frequency $f$ of the chips M57C6 and M57B2 (Purcell filter with four readout resonators) was fitted using the function [4]

$$S_{21}(f) = T_0 e^{i\phi} \frac{1}{\frac{\kappa}{2} + 2\pi i(f - f_0) + \frac{J_1^2}{\gamma_1/2 + 2\pi i(f - f_1)} + \frac{J_2^2}{\gamma_2/2 + 2\pi i(f - f_2)} + \frac{J_3^2}{\gamma_3/2 + 2\pi i(f - f_3)} + \frac{J_4^2}{\gamma_4/2 + 2\pi i(f - f_4)}} + x_0 + iy_0, \tag{2}$$

where $T_0$ gives the amplitude, $\phi$ a correcting rotation in the complex plane, $f$ the frequency of the incoming signal, $\kappa$ the full width at half maximum (FWHM), $f_0$ the resonance frequency of the Purcell filter, $J_{1,2,3,4}$ the coupling strengths of the Purcell filter and readout resonator R1 to R4 respectively, $\gamma_{1,2,3,4}$ gives the loss coefficient of the corresponding readout resonator and $f_{1,2,3,4}$ the resonance frequency of the corresponding readout resonator. The parameters $x_0$ and $y_0$ correct a complex offset. This function can be derived using the input-output model [5] like Patrik Caspar did in his semester thesis [4].

The initial values for the resonance frequency was taken from a power vs. frequency plot of the measured data. For the initial value of $T_0$ we used the radius of the polar plot. By continuously manipulating $\phi$ it's initial value was determined such that the shape of the real and imaginary part of the complex amplitude was the same as with the data. The initial value of $\kappa$ was figured out fitting a complex Lorentzian to the data as described later. For the coupling strengths one assumed lower values than for $\kappa$ and even lower ones for the loss coefficients. The goodness of the fits is very sensitive to the initial values, especially in the frequency range close to the readout resonators. To get good results for the parameters of the readout resonators this range was weighted by a factor of 10 higher.

To compare the goodness of the fit we looked at the adjusted $R^2$ value. This is a modification of the $R^2$ value which is defined as $R^2 = 1 - \frac{SS_{res}}{SS_{tot}}$, where $SS_{res} = \sum_i (f_i - \overline{y})^2$ is the residual sum of squared values and $SS_{tot} = \sum_i (y_i - \overline{y})^2$ the variance multiplied with the number of measurements ($y_i$: measued values at $x_i$, $f_i$: from fit predicted value at $x_i$, $\overline{y}$: mean value of $y_i$). The closer the value of $R^2$ is to 1 the better the data is fitted. Adjusted $R^2$ is defined as $1-(1-R^2)\frac{n-1}{n-p-1}$ [6], where n is the sample size and p the number of explanatory variables in the model. Again values close to 1 indicate better fits, than lower values, but the extension penalizes additional variables. This prevents unnecessary variables which only compensate statistical errors.

The adjusted $R^2$ value of the fit of M57C6 is 0.994251 and of M57B2 is 0.9959. Looking at the fit in the polar plane both seem to fit well while the remaining imperfections seem to be spurious resonances not covered by the model. A further reason is that the calibration was done at room temperature and the measurement at 4.2 K. So the cables in the dipstick are shorter than at the time of calibration.

The fitting parameters of the chips M57C6 and M57B2 are presented in Table 7. The only difference of these chips is the length of the Purcell filter (C6 has the longer one).

The Purcell filter on C6 has three wiggles, whereas on B2 are two. One can see that the resonance frequency of the readout resonators of B2 are slightly higher, than those of C6. These differences are $\Delta f_1 = 7.5 \pm 0.1$ MHz, $\Delta f_2 = 3.4 \pm 0.2$ MHz, $\Delta f_3 = 4.2 \pm 0.2$ MHz and $\Delta f_4 = 6.6 \pm 0.3$ MHz. The FWHM of M57B2 is larger by $881 \pm 4$ MHz than the FWHM of M57C6. The loss coefficients of the readout resonators are of the same order, namely at around 60 MHz. The highest and lowest deviations are 107 MHz and 33 MHz for M57C6 and 85 MHz and 54 MHz for M57B2. These values are 20 times smaller than $\kappa$ of M57C6 and around 40 times smaller than $\kappa$ of M57B2. They are also smaller than the coupling coefficients, which are between 112 and 259 MHz for M57C6 and between 101 and 169 MHz for M57B2. Compared to them the loss coefficients are around 2-3 times smaller. The values of the loss coefficient are the biggest for readout resonator R4 followed by R3, R2 and R1 on both chips. The coupling coefficients ordered (highest to lowest) are R4, R3, R1 and R2 for M57C6 and R4, R1, R3 and R2 for M57B2. The difference between the highest and lowest value is a factor of around 2. It is not because of different coupling capacitances at the readout resonators but due to the electric field distribution in the Purcell filter. Since the frequency is close to the resonance frequency of the Purcell filter there are standing waves in the resonator. Hence the electric field at the outer readout resonators is higher and the coupling stronger. Since the coupling resonators at the input and output port of the Purcell filter are not the same, the field is not symmetrically distributed. So the readout resonators closer to the output are coupled stronger. This means we can order the readout resonators by their expected coupling strength starting with the highest: R4, R1, R2, R3. This explains the ratio of R1, R2 and R4 but we do not know why R3 is measured to be so large.

The readout resonators were also investigated in more detail. Therefore we looked only at their resonance curve and used Equation 4 and the corresponding fitting method described below. The results can be seen in Table 8. In comparison to the results in Table 7 the values of the resonance frequencies are up to 0.002 GHz lower and their errors are smaller by a factor of up to 10. The quality factor of the readout resonators on M57C6 are between 600 and 700 while the ones of M57B2 are between 390 and 600.

The measured complex amplitude S(2,1) depending on the frequency $f$ of the Purcell filter on the chips M57A3, M57A4, M57B1 and M57F3 was fitted using the complex Lorentzian

$$S_{21}(f) = T_0 e^{i\phi} \left( \frac{1}{4Q^2 \left(\frac{f}{f_0} - 1\right)^2 + 1} + x_0 + -i \left( \frac{2Q \left(\frac{f}{f_0} - 1\right)}{4Q^2 \left(\frac{f}{f_0} - 1\right)^2 + 1} + y_0 \right) \right), \quad (3)$$

where $f_0$ is the resonance frequency, $Q$ the quality factor, $T_0$ the amplitude, $\phi$ a phase shift and $x_0 + iy_0$ a complex offset.

| | M57C6 | M57B2 |
|---|---|---|
| length of the Purcell filter in µm | 7790 | 6926 |
| $f_0$ in GHz | $6.5629 \pm 0.0002$ | $7.3126 \pm 0.0004$ |
| $f_1$ in GHz | $7.0092 \pm 0.0001$ | $7.0167 \pm 0.0001$ |
| $f_2$ in GHz | $7.0990 \pm 0.0002$ | $7.1024 \pm 0.0001$ |
| $f_3$ in GHz | $7.1717 \pm 0.0002$ | $7.1759 \pm 0.0001$ |
| $f_4$ in GHz | $7.2547 \pm 0.0003$ | $7.26132 \pm 0.00006$ |
| $\kappa/2\pi$ in MHz | $211.0 \pm 0.3$ | $350.9 \pm 0.6$ |
| $T_0$ | $0.2960 \pm 0.0004$ | $0.722 \pm 0.001$ |
| $\phi$ | $1.703 \pm 0.001$ | $3.409 \pm 0.002$ |
| $\gamma_1/2\pi$ in MHz | $7.2 \pm 0.3$ | $8.6 \pm 0.3$ |
| $\gamma_2/2\pi$ in MHz | $5.3 \pm 0.5$ | $9.1 \pm 0.3$ |
| $\gamma_3/2\pi$ in MHz | $11.6 \pm 0.6$ | $12.3 \pm 0.3$ |
| $\gamma_4/2\pi$ in MHz | $17.2 \pm 0.9$ | $13.5 \pm 0.2$ |
| $J_1/2\pi$ in MHz | $27.1 \pm 0.3$ | $22.9 \pm 0.3$ |
| $J_2/2\pi$ in MHz | $17.8 \pm 0.6$ | $16.1 \pm 0.2$ |
| $J_3/2\pi$ in MHz | $32.6 \pm 0.6$ | $21.5 \pm 0.2$ |
| $J_4/2\pi$ in MHz | $41.2 \pm 0.8$ | $27 \pm 1$ |
| $x_0$ | $0.0060 \pm 0.0001$ | $0.0569 \pm 0.0004$ |
| $y_0$ | $0.0596 \pm 0.0001$ | $0.0245 \pm 0.0004$ |

Table 7: Fitting parameters of Equation 2 and standard error of the chips M57C6 and M57B2, measured at a temperature of 4.2 K.

The maximum of the absolute value of the amplitude was determined to use its value as initial value for $T_0$ and its frequency as initial value for $f_0$. The starting value of $Q$ was determined using the formula $Q = \frac{f_0}{\delta f}$ with the initial value of $f_0$ for $f_0$ and $\delta f$ determined by the 3 dB point. The starting value of $\phi$ was chosen to be $-\mathrm{Arg}(\mathrm{mean}[\Re(data)] + i\mathrm{mean}[\Im(data)])$. For $x_0$ and $y_0$ a starting value of 0 was used. In Figure 5 a) one can see an exemplary fit for the Purcell filter on chip M57A3.

Besides this fitting function a further technique was used. As described in [3] a circle is fitted to the data in the polar plane, whereby the weighting function $W(f) = ((x_{ref} - \Re[A(f)])^2 + (y_{ref} - \Im[A(f)])^2)$ is used. In this function $x_{ref}$ and $y_{ref}$ are the real and imaginary part of the point midway between the first and the last point of the data. Then the data points are rotated and translated such that the center lies at the origin of the polar plane. Then the phase $\Phi$ depending on the frequency $f$ is fitted to the function [3]

$$\Phi(f) = 2\arctan\left(2Q\left(1 - \frac{f}{f_0}\right)\right) + f\tau + \Phi_0, \tag{4}$$

| | M57C6 | M57B2 |
|---|---|---|
| $f_1$ in GHz | $7.00847 \pm 0.00002$ | $7.0144 \pm 0.0001$ |
| $f_2$ in GHz | $7.09695 \pm 0.00002$ | $7.10121 \pm 0.00008$ |
| $f_3$ in GHz | $7.1684 \pm 0.0001$ | $7.17527 \pm 0.00004$ |
| $f_4$ in GHz | $7.25358 \pm 0.00005$ | $7.25808 \pm 0.00007$ |
| $Q_1$ in GHz | $636 \pm 8$ | $523 \pm 16$ |
| $Q_2$ in GHz | $635 \pm 8$ | $580 \pm 2$ |
| $Q_3$ in GHz | $680 \pm 5$ | $499 \pm 6$ |
| $Q_4$ in GHz | $611 \pm 9$ | $393 \pm 5$ |

Table 8: Resonance frequencies $f$ and quality factor $Q$ of the readout resonators on the chips M57C6 and M57B2. Values are determined by fitting only the single resonance curves. Errors result from fitting in different ranges and taking the average. Measurements were performed at a temperature of 4.2 K.

where $f_0$ gives the resonance frequency, $Q$ the quality factor, $\tau$ the phase delay caused by uncalibrated cables and $\Phi_0$ an offset.

The starting value of $f_0$ is the intersection of the phase with the x-axis and for $Q$ we used the value determined by the complex Lorentzian fit. The starting values of $\tau$ and $\Phi_0$ were 0. To receive good fits it is crucial to choose appropriate initial values, especially for $Q$. In Figure 5 b) one can see an exemplary fit for the Purcell filter on chip M57A3.

For both methods the fitting was performed for different ranges and the average was taken. The given errors are the standard deviations of the single fitting results.

The results for the Purcell filter of the chips M57A3, M57A4, M57B1 and M57F3 are presented in Table 9. The values of adjusted $R^2$ are slightly higher for the phase fit than for the complex Lorentzian fit. This means that the former model fits the measured data better. This is especially the case for the measurement of chip M57B1. Here the data is more noisy and the adjusted $R^2$ is smaller than in the other measurements. This might indicate that the phase is less affected by noise than the amplitude and therefore the results of the phase fit might be better than the one of the complex Lorentzian fit. Paul J. Petersan and Steven M. Anlage compared different fitting methods for determining the quality factor $Q$ and the resonance frequency of a resonator and it appears that the phase fit delivers the best accuracy for fixed input power [3]. However, in this paper the complex Lorentzian fit used here was not discussed, but a Lorentzian fit of the absolute value and several fits in the complex plane. Thus the phase fit was used for the following comparison of the fitting results and for the overview of the results.

In Table 9 one can see that the resonance frequencies determined by the Lorentzian fit and by the phase fit are almost the same. The relative differences (assuming the phase fit is correct) are 0.0002%, 0.03%, 0.0001% and 0.01% for the chips M57A3, M57A4, M57B1

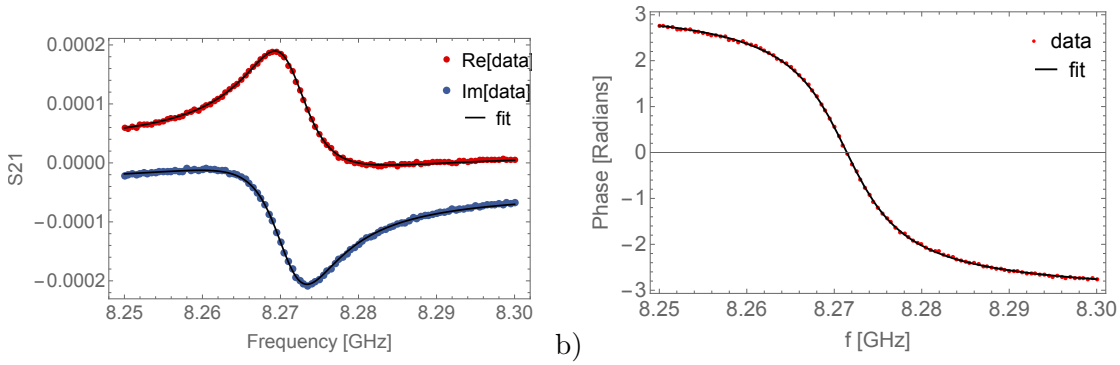


Figure 5: Transmission coefficient through an under-coupled Purcell filter type resonator: a) Real and imaginary part of the transmission amplitude and a complex Lorentzian fit. b) Phase of the transmission and a phase fit. These values were measured at a temperature of 4.2 K for chip M57A3.

and M57F3 respectively. M57A3 and M57B1 have the same length but on M57A3 there are also T-junctions resulting in a 320 MHz lower resonance frequency. The length of M57A4 and M57B1 are approximately the same but the coupling capacitance of M57A4 is higher and hence its resonance frequency is lower (by about 920 MHz). For $Q$ the relative differences are larger: 1%, 3%, 2% and 5%. The quality factor of the over-coupled Purcell filter (M57A4) is much lower (factor of 20 to 50) than the one of the under-coupled Purcell filters (M57A3, M57B1 and M57F3).

The shape of transmission amplitude of the coupling resonators on the chips M57A3, M57A4, M57B1 and M57F3 is a Fano resonance caused by an interference with another resonance (Table 6). Thus the measured complex amplitude S(2,1) depending on the frequency $f$ was fitted using the asymmetrical fit function

$$S_{21}(f) = T_0 e^{i\phi}\left(1 - \frac{Q\left(1+\frac{2iQ(f_1-f_0)}{f_0}\right)}{Q_e\left(1+\frac{2iQ(f-f_0)}{f_0}\right)} + x_0 + iy_0\right) \text{[7]}. \tag{5}$$

$T_0$ is the amplitude, $\phi$ a phase shift, $f_0$ the resonance frequency, $Q$ the quality factor, $f_1$ the frequency where the imaginary part vanishes (quantifies the asymmetry) and $Q_e$ the external Quality factor. $x_0 + iy_0$ is an offset. The fit was weighted like it was done for the phase fit.

We used the radius of the polar plot as initial value for $T_0$ and $-\text{Arg}(\text{mean}[\Re(data)] + i\text{mean}[\Im(data)])$ for $\phi$. A good starting value of $f_0$ was determined using the power vs. frequency plot. For $Q$ we tried several guesses to find a appropriate initial value. For the offset $x_0 + iy_0$ the initial value 0 was chosen. It was not possible to find numerically stable initial values for $Q_e$ and $f_1$. We found good fits for each order of magnitude of $Q_e$ from

| | M57A3 | M57A4 | M57B1 | M57F3 |
|---|---|---|---|---|
| resonator length in µm | 7306 | 7386 | 7306 | 5884 |
| $C_{in}/C_{out}$ in fF | 0.32/0.32 | 25/120 | 0.32/0.32 | 0.32/0.32 |
| $f_0$ in GHz (complex Lorentzian fit) | $8.27122 \pm 0.00003$ | $7.570 \pm 0.007$ | $8.49797 \pm 0.00009$ | $10.5807 \pm 0.0003$ |
| $f_0$ in GHz (phase fit) | $8.27124 \pm 0.00003$ | $7.572 \pm 0.002$ | $8.49807 \pm 0.0001$ | $10.582 \pm 0.001$ |
| $Q$ (complex Lorentzian fit) | $819 \pm 12$ | $22.0 \pm 0.5$ | $1101 \pm 15$ | $345 \pm 45$ |
| $Q$ (phase fit) | $810 \pm 1$ | $21.31 \pm 0.09$ | $1125 \pm 26$ | $339 \pm 25$ |
| adjusted $R^2$ (complex Lorentzian fit) | 0.99966 | 0.995998 | 0.929789 | 0.989602 |
| adjusted $R^2$ (phase fit) | 0.999958 | 0.999862 | 0.991163 | 0.998848 |

Table 9: Measured resonance frequency $f_0$ and quality factor $Q$ of the Purcell filter of the chips M57A3, M57A4, M57B1 and M57F3. Results are determined using a complex Lorentzian fit and a phase fit. The adjusted $R^2$ values of the fits are presented in the last two lines. The measurements were performed at a temperature of 4.2 K.

$10^3$ to $10^7$. This is because of the offset which gives the fit to many degrees of freedom. But the offset is necessary since some data does not cross the real axis which defines $f_1$. However, the values of $f_0$ and $Q$ were the same for the different fits with the different values of $Q_e$ and $f_1$.

The phase fit explained above was also used to fit the transmission amplitude of the coupling resonators. Examples of both can be seen in Figure 6.

In Table 10 and 11 one can see the fitting results of the coupling resonators at 8 GHz and 8.5 GHz respectively. Both resonator types are on the chips M57A3, M57A4, M57B1 and M57F3. The coupling resonator of M57B1 at 8 GHz was damaged and hence it could not be measured. The values of adjusted $R^2$ are close to 1 (lowest: 0.99929, highest: 0.99996) for both fitting methods in all measurements. The values of the phase fit are a little higher than the one of the asymmetric fit. Because of this and the fitting problems for the asymmetric fit we have chosen the phase fit method for the values given in the overview and the following differences are given relative to the phase fit.

The resonance frequency of the coupling resonator at 8 GHz on the chip M57A3 is the same within the error bounds for both fitting methods. The relative differences of this resonator on the chips M57A4 and. M57F3 are both 0.001%. The relative differences of $Q$

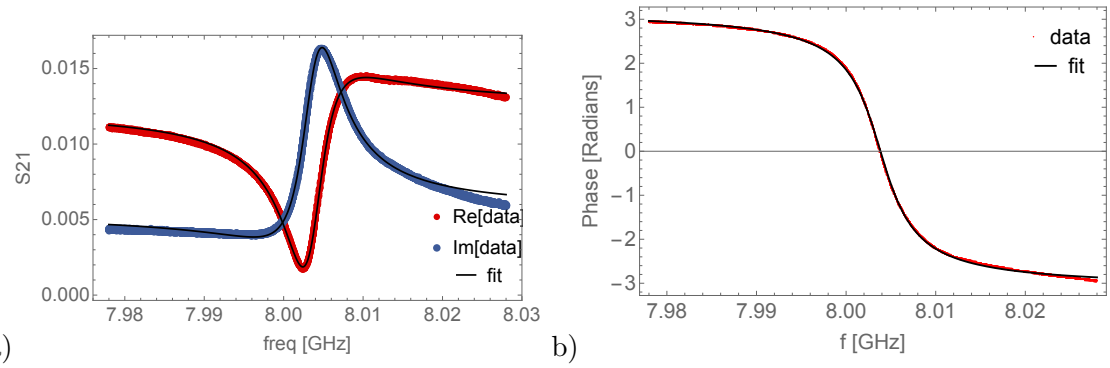


a) b)

Figure 6: Transmission coefficient through a coupling resonator: a) Real and imaginary part of the measured complex transmission amplitude S(2,1) of the coupling resonator at 8 GHz on chip M57A4 and a complex asymmetrical fit [7]. b) Phase of the transmission amplitude and a phase fit. These values were measured at a temperature of 4.2 K for chip M57A3.

are 1%, 1% and 0.6% for M57A3, M57A4 and M57F3, respectively. So the fitting results of $f_0$ are very similar and the of $Q$ differ about less than 1%. The average value and the standard deviation of the resonance frequencies is $8.0041 \pm 0.0029$ GHz and the mean of $Q$ is $1433 \pm 128$.

Now we look at the second coupling resonators on the chips M57A3, M57A4, M57B1 and M57F3. For the relative differences of the resonance frequency 0.0017%, 0.0003%, 0.0002% and 0.0012% were found respectively. For $Q$ they are 1.2%, $\approx 0$, 1.2% and 0.6%. Like we have seen for the first resonator the values of $f_0$ are very similar for both fitting methods (difference below 0.0017%) and the $Q$ differs about less than 1.2%. The mean of $f_0$ is $8.5153 \pm 0.0078$ GHz and the mean of $Q$ is $1456 \pm 87$.

**Measurements at 20 mK:** In the dilution cryostat only the absolute value of the transmission amplitude and not the phase was measured. Therefore we used a Lorentzian to fit the data. To take account of the background we used the function [3]

$$|S_{21}(f)| = A_1 + A_2 f + \frac{S_{max} + A_3 f}{\sqrt{4Q^2 \left(\frac{f}{f_0} - 1\right)^2 + 1}}, \tag{6}$$

where the frequency is $f$ and the fitting parameters are the resonance frequency $f_0$, quality factor $Q$, maximum magnitude $S_{max}$, constant background $A_1$, slope on the background $A_2$ and skew $A_3$. For $A_3 = 0$ this functions becomes a regular Lorentzian with background. The data was fitted using this fit function with several combinations of the $A_i$, i = 1,2,3: without $A_i$, only with $A_3$, with $A_1$ and $A_2$ and with $A_1$, $A_2$ and $A_3$.

| | M57A3 | M57A4 | M57B1 | M57F3 |
|---|---|---|---|---|
| $f_0$ in GHz (asymmetrical fit) | 8.001435 ± 0.000006 | 8.003691 ± 0.000001 | - | 8.007044 ± 0.000002 |
| $f_0$ in GHz (phase fit) | 8.001432 ± 0.000006 | 8.003774 ± 0.000001 | - | 8.007148 ± 0.000002 |
| $Q$ (asymmetrical fit) | $1564 \pm 4$ | $1365 \pm 1$ | - | $1376 \pm 1$ |
| $Q$ (phase fit) | $1581 \pm 4$ | $1351 \pm 1$ | - | $1368 \pm 1$ |
| adjusted $R^2$ (asymmetrical fit) | 0.99929 | 0.999877 | - | 0.999771 |
| adjusted $R^2$ (phase fit) | 0.999881 | 0.999889 | - | 0.999909 |

Table 10: Measured resonance frequency $f_0$ and quality factor $Q$ of the coupling resonator at 8 GHz of the chips M57A3, M57A4, M57B1 and M57F3. Results are determined using a complex Lorentzian fit and a phase fit. The adjusted $R^2$ values of the fits are presented in the last two lines. The measurements were performed at a temperature of 4.2 K.

The initial value of $f_0$ and $S_{max}$ was determined by the maximum of the data and the starting value of $Q$ was found in the same way as for the complex Lorentzian fit using the 3 dB point. For $A_1$, $A_2$ and $A_3$ we used an initial value of 0.

In the dilution cryostat (20 mK) we measured the Purcell filter of M57A3 and M57B1 as well as the coupling resonator at 8 GHz on M57A3. These measurements were performed for different input powers to investigate the dependency of $Q$ on the number of photons in the resonator. Mean, minimum and maximum of adjusted $R^2$ were determined for comparison of the goodness of fit between the fitting models. The values of M57B1 are presented in Table 12. The mean, minimum and maximum of adjusted $R^2$ are closest to 1 for a fit with $A_1$, $A_2$ and $A_3$ followed by a fit using $A_1$ and $A_2$, a fit using $A_3$ and the lowest values were determined for the Lorentzian fit without corrections. The values of adjusted $R^2$ are all close to 1 which means that the data is fitted well. Comparing the determined $Q$ (Figure 7) one can recognize that the fitting methods using the background corrections $A_1$ and $A_2$ have large errors in $Q$. However, the other methods do not have this problem. Thus the Lorentzian fit with only skew $A_3$ is assumed to give the best results for $Q$.

For the mean resonance frequencies all fitting methods gave the same value up to an error of order $10^{-6}$ GHz. The results are $8.3102138 \pm (7 \times 10^{-7})$ GHz (Purcell filter M57A3), $8.5132131 \pm (7 \times 10^{-7})$ GHz (Purcell filter M57B1) and $8.031852 \pm (2 \times 10^{-6})$ GHz (coupling resonator M57A3). Compared to the measurements with the dipstick at 4.2 K they are about 0.04, 0.015 and 0.03 GHz higher. Measuring with an input power (at the resonator) of -94 dBm we found a quality factor of $253000 \pm 6000$, $145000 \pm 1000$ and $102500 \pm 300$, respectively. Thus they are larger by a factor of around 320, 130 and

| | M57A3 | M57A4 | M57B1 | M57F3 |
|---|---|---|---|---|
| $f_0$ in GHz (asymmetrical fit) | 8.513553 ± 0.000005 | 8.513136 ± 0.000001 | 8.526534 ± 0.000001 | 8.508083 ± 0.000002 |
| $f_0$ in GHz (phase fit) | 8.513412 ± 0.000004 | 8.513109 ± 0.000001 | 8.526521 ± 0.000001 | 8.508189 ± 0.000002 |
| $Q$ (asymmetrical fit) | $1429 \pm 2$ | $1537.2 \pm 0.4$ | $1483.1 \pm 0.5$ | $1330 \pm 1$ |
| $Q$ (phase fit) | $1446 \pm 2$ | $1537.2 \pm 0.7$ | $1500.9 \pm 0.6$ | $1338 \pm 1$ |
| adjusted $R^2$ (asymmetrical fit) | 0.999358 | 0.999959 | 0.999863 | 0.999748 |
| adjusted $R^2$ (phase fit) | 0.999757 | 0.99996 | 0.999955 | 0.999875 |

Table 11: Measured resonance frequency $f_0$ and quality factor $Q$ of coupling resonator at 8.5 GHz of the chips M57A3, M57A4, M57B1 and M57F3. Results are determined using a complex Lorentzian fit and a phase fit. The adjusted $R^2$ values of the fits are presented in the last two lines. The measurements were performed at a temperature of 4.2 K.

| M57B1 | Mean(adjusted $R^2$) | Min(adjusted $R^2$) | Max(adjusted $R^2$) |
|---|---|---|---|
| without $A_i$ | 0.996881 | 0.973441 | 0.999989 |
| $A_3$ | 0.996909 | 0.973558 | 0.999993 |
| $A_1$, $A_2$ | 0.997003 | 0.974324 | 0.999994 |
| $A_1$, $A_2$, $A_3$ | 0.997047 | 0.974594 | 0.999995 |

Table 12: Mean, minimum and maximum of adjusted $R^2$ for the measurements at 20 mK of the Purcell filter on M57B1. The values are averaged over the measurement, where the input power was swept between -76 and -130 dBm in steps of 3 dBm. The fitting methods were Lorentzian fits using Equation 6.

72, respectively, than the values measured at a temperature of 4.2 K. These values for $Q$ measured in the dilution cryostat are of the same order as presented in the paper of M. Göppl [1]. Using the same coupling capacitances $C_\kappa = 0.32$ fF as in the Purcell filters he found the quality factor $Q = 2.3 \times 10^5$ which is between the value of M57A3 and M57B1. The resonance frequency of this resonator was $f_0 = 2.3459$ GHz.

The formula

$$n = \frac{P_{in} Q^2}{2\pi^2 \hbar f_0^2 Q_e} \tag{7}$$

gives an estimate of the number of photons $n$ in a resonator depending on the input power $P_{in}$, the quality factor $Q$, the resonance frequency $f_0$ and the external quality factor $Q_e$ of the resonator. The external quality factor was determined by simulation (see below). In

Figure 7 b) and 8 one can see the quality factor $Q$ depending on the number of photons in the resonator. For the Purcell filter $Q$ seems to approach a limit of around $180000 \pm 10000$ (M57A3) and $120000 \pm 10000$ (M57B1) for $n < 100$. For larger numbers of photons $Q$ is increasing to $293000 \pm 8000$ (14000000 photons) and $154200 \pm 300$ (3700000 photons), respectively. From the measurement of M57B1 one can determine the effective permittivity $\epsilon_{eff}$ using the formula

$$f_0 = \frac{c}{\sqrt{\epsilon_{eff}} 2l}, \tag{8}$$

where $c$ is the speed of light and $l$ the length of the resonator. This results in $\epsilon_{eff} = 5.83$. In earlier measurements one found $\epsilon_{eff} = 5.67$.

For the coupling resonator $Q$ seems to converge to 105000 for photon numbers $n > 8000$. Lowering the number of photons in the resonator $Q$ decreases to $64000 \pm 5000$ (around 2 photons). The transmission curve which belongs to this $Q$ has a worse signal to noise ratio which lends to a larger error in the fit.

In comparison to the measurements at a temperature of 4.2 K the shape of the resonance is not a Fano resonance. Probably the reason is that at the lower temperature the quality factor is higher and therefore the resonance peak is more narrow(smaller frequency range). Thus the background affects the resonance less and the shape is a Lorentzian.

**Simulations**

To predict and design the resonance frequencies of the resonators, simulations were performed using the software AWR Microwave Office. In Figure 9 a) one can see the circuit layout for the Purcell filter simulations where $C_{in}$ and $C_{out}$ are the appropriate capacitances at the in- and output. Figure 9 b) shows the layout for the coupling resonators. Since here relative large pads are used for the coupling we also had to take the capacitance to the ground into account. The circuit layout of the chips M57B2 and M57C6 are presented in Figure 10. Here we simulated the Purcell filter coupled to the readout resonators by pads with the capacitance $C_{ROtPF} = 20\,\text{fF}$. The capacitances of the pads connecting the coupling resonators and the readout resonators to the qubits were determined using the simulation software Ansys Maxwell. This yielded $C_{ground}^{couplingRes} = 64.5\,\text{fF}$ for the capacitance of the coupling resonator pad to ground, $C_{\kappa}^{couplingRes} = 1.5\,\text{fF}$ for the capacitance at the in/output of the readout resonator and $C_{QubitCap} = 0.445\,\text{fF}$ for the capacitance of the readout resonator pad to the qubit.

The simulations of the resonators were performed for $\epsilon_{eff}^{(1)} = 5.67$ and $\epsilon_{eff}^{(2)} = 5.83$ to get the transmission amplitude S(2,1). The data was fitted using the same methods as for the measured data. The fitting parameters for the chips M57C6 and M57B2 are presented in Table 13. The simulated resonance frequencies are lower for $\epsilon_{eff}^{(2)}$ than for $\epsilon_{eff}^{(1)}$, which can be explained by the Equation 8. This difference is about 70 and 90 MHz for the Purcell filter and readout resonator, respectively. Comparing the simulation for $\epsilon_{eff}^{(1)}$ with the simulation for $\epsilon_{eff}^{(2)}$, the value of $\kappa$ is about 3% smaller.

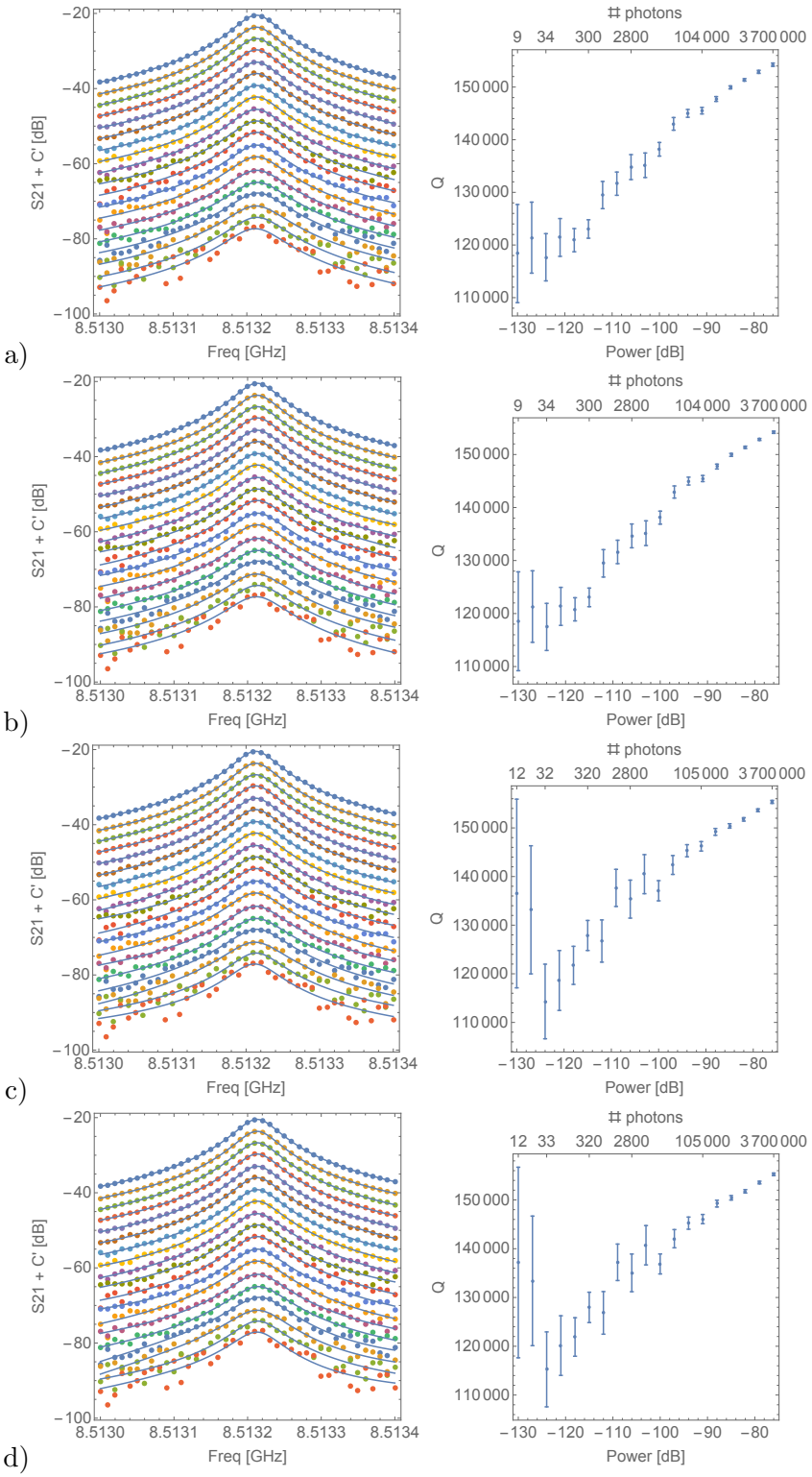


Figure 7: Purcell filter of M57B1 in the dilution cryostat at 20 mK: Transmission coefficient depending on the frequency for different input powers between -76 dBm (highest curve) and -130 dBm (lowest curve) in steps of 3 dBm on the left side and a Q vs. number of photons plot on the right side. a) Fit without $A_1$, $A_2$ and $A_3$. b) Fit with $A_3$. c) Fit with $A_1$ and $A_2$. d) Fit with $A_1$, $A_2$ and $A_3$.

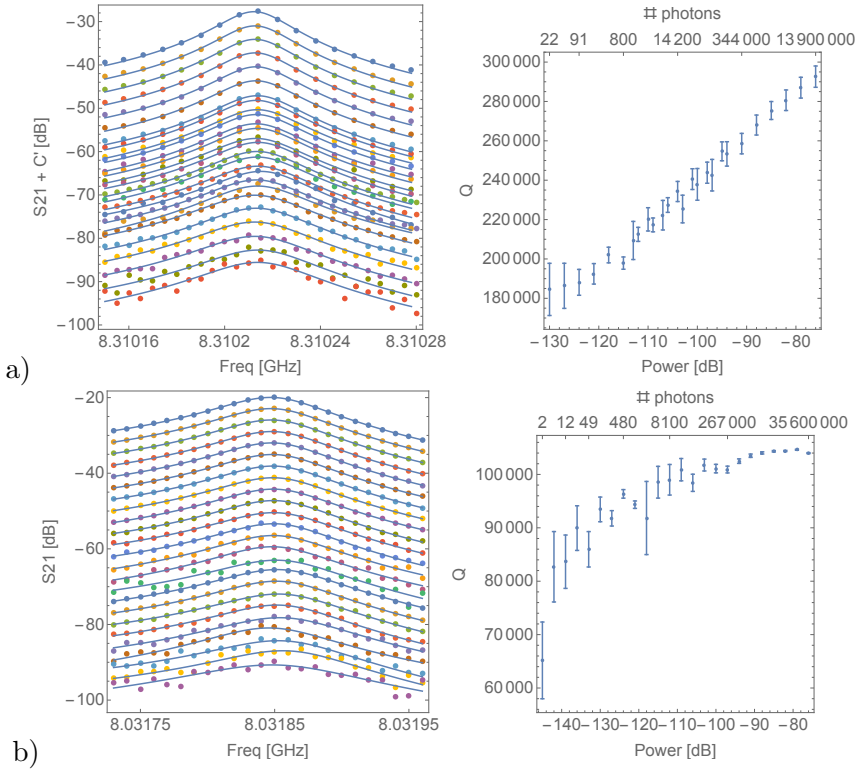


Figure 8: Measurements of a) the Purcell filter and b) the coupling resonator in the dilution cryostat at 20 mK: Transmission coefficient depending on the frequency for different input powers between -76 dBm (highest curve) and -130 dBm for a) (-145 dBm for b)) (lowest curve) on the left side and a Q vs. number of photons plot on the right side. Fits are done with $A_3$.

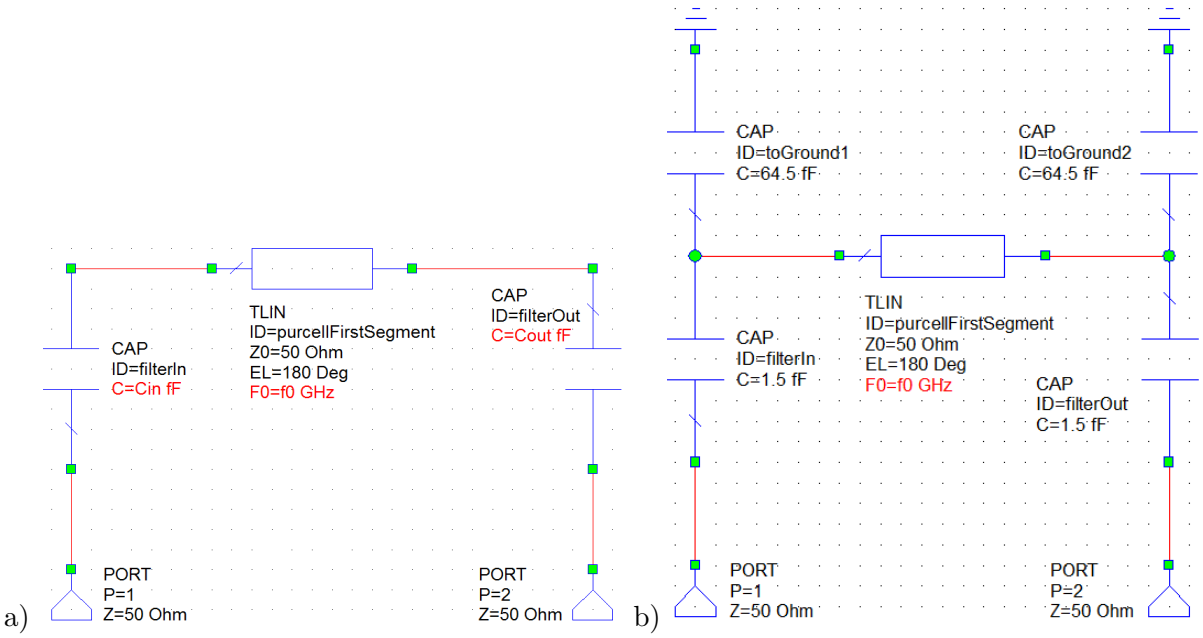


Figure 9: a) Circuit layout for the simulations of the Purcell filter and b) for the simulations of the coupling resonators.

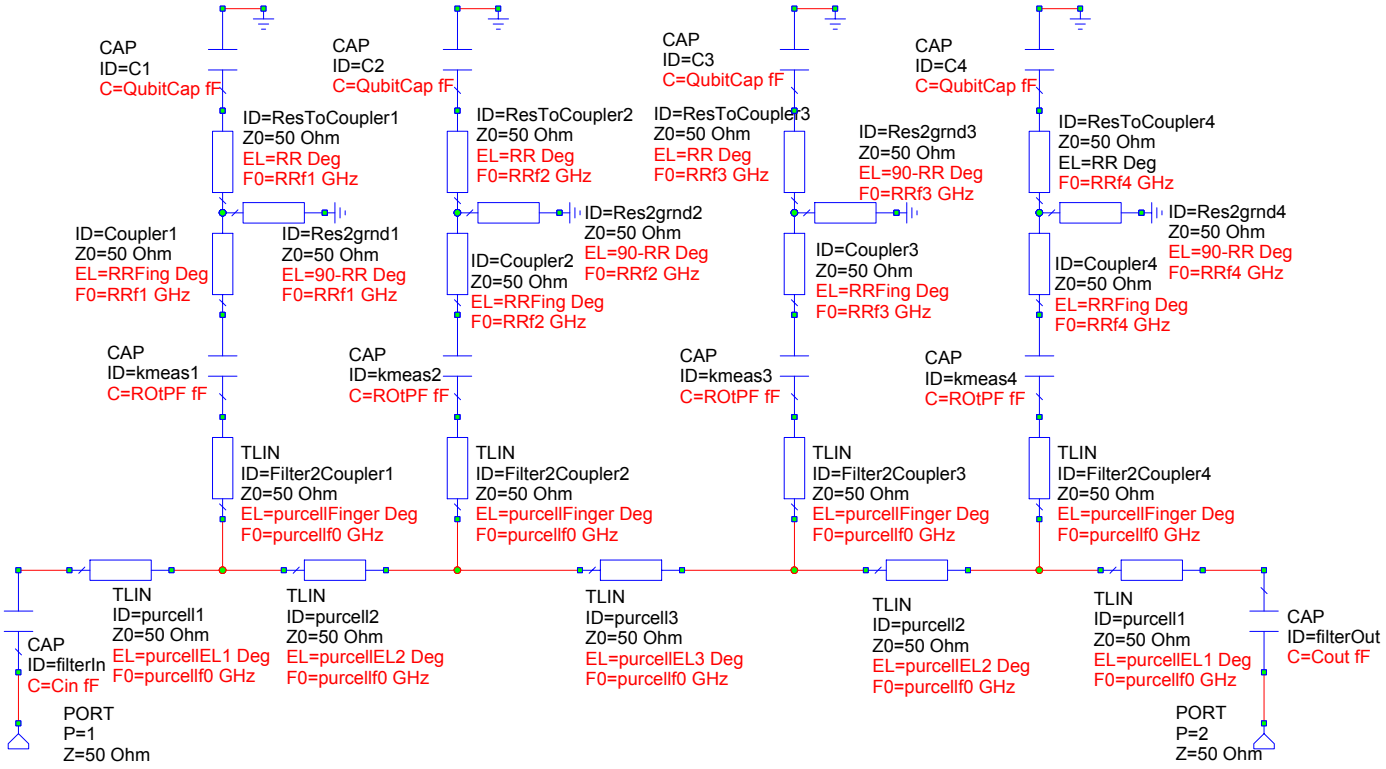


Figure 10: Circuit layout for the simultions of M57C2 and M57C6. In the lower part the Purcell filter is located while the readout resonators are in the middle and upper part. They are numbered from left to right and not by the value of their resonance frequency. In the notation introduced in Table 1 the names are R1, R3, R2 and R4 (from left to right).

| | **M57C6** (Purcell filter length: 7790 µm) | | | **M57B2** (Purcell filter length: 6926 µm) | | |
|---|---|---|---|---|---|---|
| | simulated using $\epsilon_{eff}^{(1)}$ | simulated using $\epsilon_{eff}^{(2)}$ | measured data | simulated using $\epsilon_{eff}^{(1)}$ | simulated using $\epsilon_{eff}^{(2)}$ | measured data |
| $f_0$ | 6.6654 | 6.5945 | $6.5629 \pm 0.0002$ | 7.3945 | 7.3170 | $7.3126 \pm 0.0004$ |
| $f_1$ | 7.0713 | 6.9869 | $7.00847 \pm 0.00002$ | 7.0714 | 6.9866 | $7.0144 \pm 0.0001$ |
| $f_2$ | 7.1521 | 7.0668 | $7.09695 \pm 0.00002$ | 7.1524 | 7.0670 | $7.10121 \pm 0.00008$ |
| $f_3$ | 7.2304 | 7.1442 | $7.1684 \pm 0.0001$ | 7.2306 | 7.1443 | $7.17527 \pm 0.00004$ |
| $f_4$ | 7.3114 | 7.2242 | $7.25358 \pm 0.00005$ | 7.3116 | 7.2244 | $7.25808 \pm 0.00007$ |
| $\kappa$ | 1.436 | 1.395 | $1.324 \pm 0.002$ | 1.887 | 1.826 | $2.205 \pm 0.004$ |

Table 13: Simulated and measured resonance frequency of the Purcell filter $f_0$ and of the readout resonators $f_1$, $f_2$, $f_3$ and $f_4$ as well as the FWHM $\kappa$. Simulations were performed for the effective permittivities $\epsilon_{eff}^{(1)}$ and $\epsilon_{eff}^{(2)}$.

Now we analyse M57C6. For the Purcell filter both simulated values of the resonance frequency are too large but the second simulation ($\epsilon_{eff}^{(2)}$) is closer to the measured data. They differ about 0.5%. Looking at the readout resonators one finds that the first simulation yields larger values and the second simulations lower values compared to the measured data. Again $\epsilon_{eff}^{(2)}$ leads to results closer to the measurement differing about 0.3% ($f_1$), 0.4% ($f_2$), 0.3% ($f_3$) and 0.4% ($f_4$). For the value of $\kappa$ the second simulation is closer to the measurement, too.

For M57B2 similar results were obtained. The resonance frequency of the Purcell filter determined by the simulation using $\epsilon_{eff}^{(2)}$ is very close to the measured value (difference: 0.05%, whereas the resonance frequency of the first simulations is 1.1% larger. Investigating the readout resonator frequencies one sees that again the second simulation matches the observed results better than the first simulation. The differences between the former and the measured data are 0.4% ($f_1$), 0.5% ($f_2$), 0.4% ($f_3$) and 0.5% ($f_4$). However, the value of $\kappa$ is simulated better by the first simulation but here the differences are high: 14%.

In summary, the simulation using $\epsilon_{eff}^{(2)}$ gives better predictions for the resonance frequencies. The difference between the simulated and measured frequencies is around 0.4%.

The readout resonators on both chips have resonance frequencies of M57B2 which are higher than those of M57C6 except for $f_1$ determined with $\epsilon_{eff}^{(2)}$. But these differences are small, around 0.004%. The measured readout resonance frequencies of M57B2 are around 0.04 to 0.1% percent higher. This might occur because of measurement errors.

In Table 14 the fitting parameters of the coupling resonators and of the Purcell filters on the chips M57B1, M57A4 and M57F3 are presented. The Purcell filter on M57A3 is the same as M57B1 with the difference that the resonator on M57A3 is extended by T-junctions. This leads to a lower resonance frequency $f_0$.

For the coupling resonators as well as for M57F3 both fitting methods (complex Lorentzian fit and phase fit) result in the same $f_0$ and $Q$ up to the given accuracy. $Q$ and $f_0$ of M57B1 differ about 0.0037% and 0 (up to given accuracy), respectively, while these values of M57A4 differ about 1% and 0.005% for both $\epsilon_{eff}$. Since the values of adjusted $R^2$ of the phase fit are always higher (it was 1 except for M57B1 where it was 0.999998) than for the Lorentzian fit, the values of the phase fit are presented in the Table 14. Since this simulations were performed with lossless elements, the internal quality factor $Q_i$ was assumed to be high compared to the external quality factor $Q_e$. This means that the simulated values of $Q$ are the values of $Q_e$ because of $\frac{1}{Q} = \frac{1}{Q_e} + \frac{1}{Q_i}$.

For the Purcell filter on M57A4 the values of $Q$ are very similar but the simulation with $\epsilon_{eff}^{(2)}$ is closer to the measured value, 1.2% difference. This means that the measured value of $Q$ is very close to $Q_e$ and therefore $Q_i$ is much greater than $Q_e = 20.95$.

For the Purcell filter on M57B1 and M57F3 as well as for the coupling resonators the values of $Q_e$ are much higher than the one of M57A4. The reason is that these resonators are under-coupled ($C_\kappa = 0.32\,\mathrm{fF}$) but the Purcell filter on M57A4 is coupled stronger. Thus the relation $Q_e << Q_i$ does not hold for these resonators and the measured values differ a lot from the simulated. For the coupling resonator at 8 GHz $Q_e = 56760$ was found but in the dilution cryostat (20 mK) we measured $Q \sim 100000 > Q_e$. Thus the simulation is not totally correct and should be improved. Probably the coupling capacitances should be corrected.

The simulated values of $Q_e$ are used for the $Q$ vs. number of photons plot as explained above and can be used to calculate

$$Q_i = 1/(\frac{1}{Q} - \frac{1}{Q_e}). \tag{9}$$

The results can be seen in Table 15. The calculations were done using the $Q_e$ values from the $\epsilon_{eff}^{(2)}$ simulation. Since $Q$ is too close to $Q_e$ in the measurement of M57A4 one does not obtain a proper result for $Q_i$. Looking at formula 9 one recognizes that small variations of the denominator change $Q_i$ a lot because of $Q \approx Q_e$. But if we assume the internal quality factor of M57A4 to be the same as the of M57B1 (most similar chip) we find for the quality factor $Q = 20.6$ which is close to the measured value $Q = 21.31$. Thus this seems to be a reasonable assumption.

The insertion loss $L_0$ can be calculated using the formula [1]

$$L_0 = -10\log_{10}(\frac{g}{g+1})^2\ \mathrm{dB} \quad \text{with} \quad g = Q_i/Q_e. \tag{10}$$

For $Q_i << Q_e$ it holds $Q_i \approx Q$ and hence the formula for the insertion loss simplifies to $L_0 = -20\log_{10}(\frac{Q}{Q_e})$. This formula was used for the Purcell filters on M57A3, M57B1 and

| | M57A4 PF | M57B1 PF | M57F3 PF | coupling Resonator at 8 GHz | coupling Resonator at 8.5 GHz |
|---|---|---|---|---|---|
| over-coupled resonator | $\surd$ | X | X | X | X |
| $f_0^{data}$ in GHz | 7.572 $\pm$ 0.002 | 8.49807$\pm$ 0.0001 | 10.582 $\pm$ 0.001 | $8.0041 \pm 0.0029$ | $8.5153 \pm 0.0078$ |
| $f_0^{sim,\,\epsilon_{eff}^{(1)}}$ in GHz | 7.6431 | 8.61153 | 10.6910 | 8.0806 | 8.5924 |
| $f_0^{sim,\,\epsilon_{eff}^{(2)}}$ in GHz | 7.5601 | 8.50866 | 10.5633 | 7.9940 | 8.5009 |
| $Q^{data}$ | 21.31 $\pm$ 0.09 | 1125$\pm$26 | $339 \pm 25$ | $1433 \pm 128$ | $1456 \pm 87$ |
| $Q^{sim,\,\epsilon_{eff}^{(1)}}$ | 20.55 | $1.048 \times 10^6$ | 679918 | 55578 | 49312 |
| $Q^{sim,\,\epsilon_{eff}^{(2)}}$ | 20.95 | $1.073 \times 10^6$ | 696454 | 56760 | 50350 |

Table 14: Measured and simulated (for both $\epsilon_{eff}$) resonance frequency $f_0$ and quality factor $Q$ of the Purcell filters (PF) and coupling resonators. For the latter the shown values for the data are the mean values of the measurements.

M57F3 as well as for the coupling resonators. For M57A4 one assumes $Q_i$ to be the same as for M57B1: $Q_i = 1125$. The results for $L_0$ are presented in Table 15. The highest $L_0$ was observed for M57F3 ($\approx$ 66 dB) and the lowest for M57A4 (0.16 dB). All under-coupled Purcell filter have an insertion loss of around 62 dB and the coupling resonators of around 31 dB.

For the Purcell filter the insertion loss can be compared with $-S_{21}(f_{res})$. This value is value is always above the $L_0$ value thus there are additional losses like the PCB cables. For the Purcell filters on M57A3, M57B1 and M57F3 the differences are close to 10 dB and for the one on M57A4 the difference is around 2.3 dB. But for this measurement we had to correct the data using the measurement of a through plug like it is described in chapter 3. This might explain why here the value is different.

For the measurements at 20 mK there was no information about the gain in the measurement apparatus.

### Cross Talk

To analyse the influence of the resonators on each other, the transmission through the ports of different resonators is looked at.

The crosstalk of M57C6 can be seen in Figure 11, where S(2,5) is the transmission used for the qubit readout. It is around 25 dBm higher than the transmission between the charge line and the ports of the Purcell filter (S(3,5) and S(3,2)) and the transmission

| | PF M57A3 | PF M57A4 | PF M57B1 | PF M57F3 | CR at 8 GHz | CR at 8.5 GHz |
|---|---|---|---|---|---|---|
| $Q_i$ at 4.2 K | $811 \pm 1$ | - | $1126 \pm 26$ | $339 \pm 25$ | $1470 \pm 135$ | $1499 \pm 92$ |
| $Q_i$ at 20 mK | $220000 \pm 20000$ | - | $132000 \pm 1100$ | - | - | - |
| $L_0$ in dB at 4.2 K | $62.44 \pm 0.01$ | $0.1603 \pm 0.0004$ | $59.6 \pm 0.2$ | $66.3 \pm 0.6$ | $32.0 \pm 0.8$ | $30.8 \pm 0.5$ |
| $-S_{21}(f_{res})$ in dB at 4.2 K | $72.3 \pm 0.1$ | $2.44 \pm 0.03$ | $68.9 \pm 0.1$ | $80.3 \pm 0.1$ | - | - |
| $L_0$ in dB at 20 mK | $12.5 \pm 0.2$ | - | $17.38 \pm 0.06$ | - | - | - |

Table 15: Internal quality factor $Q_i$ and insertion loss $L_0$ of the Purcell filters (PF) and the coupling resonators (CR). For the Purcell filters also the values of $S_{21}(f_{res})$ are presented.

between the flux lines S(12,11). The transmission coefficient between the flux lines and the Purcell filter is even smaller by 45 dBm (S(13,2), S(11,5), S(12,5) and S(13,5)). Thus the flux and charge lines affect the transmission S(2,5) only by a little so it is not disturbed. The transmission between the neighbouring flux lines increases up to a frequency of 2 GHz and stays then at around -60 dBm. The crosstalk from the charge lines has the same position of transmission peaks as the Purcell filter and the readout resonators but the peaks of the resonators located close to the flux lines are higher since here more power can be transferred. The transmission between the flux lines and the Purcell filter is increasing with the frequency and has a resonance at 14 GHz.

In Figure 12 the crosstalk of M57B2 can be seen. Again we are mainly interested in S(2,5) and that it is not disturbed by the charge and flux lines. This applies since the other transmissions are much lower (crosstalk to charge lines by 25 dBm and flux lines by 45 dBm). The transmission form the charge lines to the Purcell filter (S(5,4) and S(5,3)) has resonances at the same frequencies as S(2,5). Similarly as for M57C6 the peaks are higher for the readout resonators located close to the charge lines. This is also the reason for the higher peaks because it allows stronger transfer. The transmission between flux line and charge line (S(3,13)) is quite low (around -80 dBm) as well as the between flux line and Purcell filter S(5,13) (around -95 dBm). The latter is influenced by the Purcell filter and the readout resonators.

The difference of the transmission coefficient through the Purcell filter and of the crosstalk to the charge lines is plotted in Figure 13. For M57C6 the differences are always below 20 dB thus the power of crosstalk is lower by a factor of 100 and the amplitude by 10. Now we look at the range from 6 to 8 GHz. One can see that the crosstalk to the input is lower than the one to the output, since there the coupling resonator is lower. Outside of the resonances the power difference is below 30 dB (crosstalk to output) and below 40 dB (crosstalk to input).

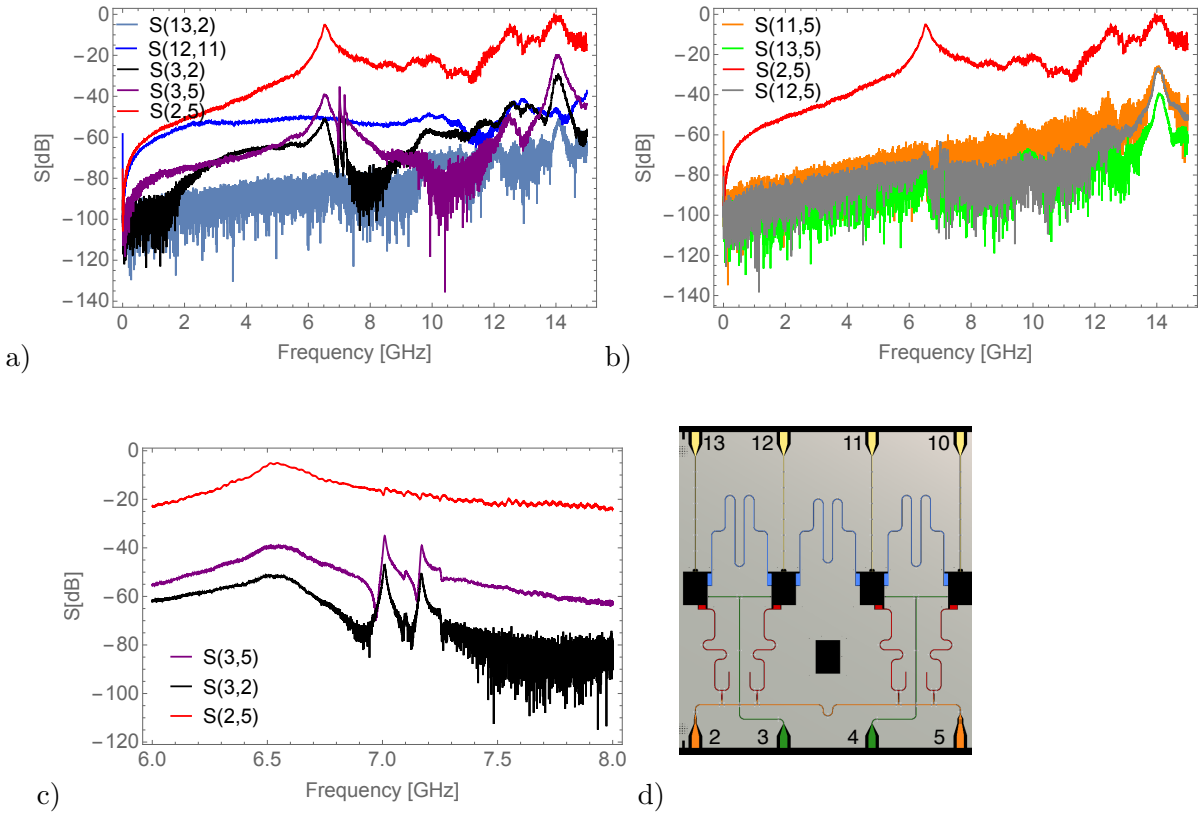


Figure 11: a), b) and c): Crosstalk of M57C6, where 2 is the input, 5 the output port, 3-4 the charge lines and 10-13 the flux lines numbered like in d). Measured at 4.2 K.

For M57B2 the differences of the transmission through the Purcell filter to the crosstalk of the output and both charge lines are depicted. Like for M57C6 the differences are below 20 dB. As already mentioned above, the resonance peaks corresponding to the readout resonators located close to the charge lines are higher. The crosstalk can be reduced by enlarging the distance of the charge lines to the readout resonators.

The crosstalk between the coupling resonators is analysed using the chips M57A4 and M57F3. S(13,12) and S(11,10) are the transmission coefficient through the coupling resonators. One can recognize the sharp resonances but the graph has other wider wiggles, especially a big one at 14 GHz. However in a smaller range around the resonance peaks the curve is more flat.

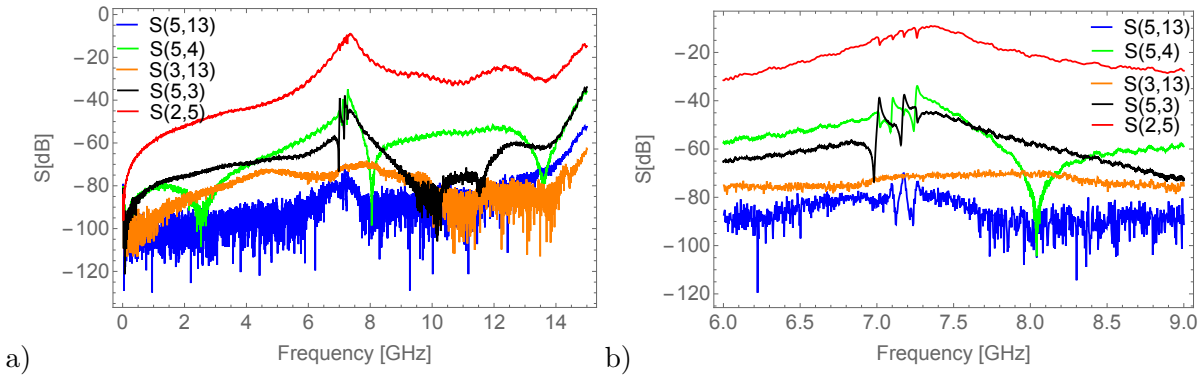


Figure 12: a) and b): Crosstalk of M57B2, where 2 is the input, 5 the output port, 3-4 the charge lines and 10-13 the flux lines. Measured at 4.2 K.

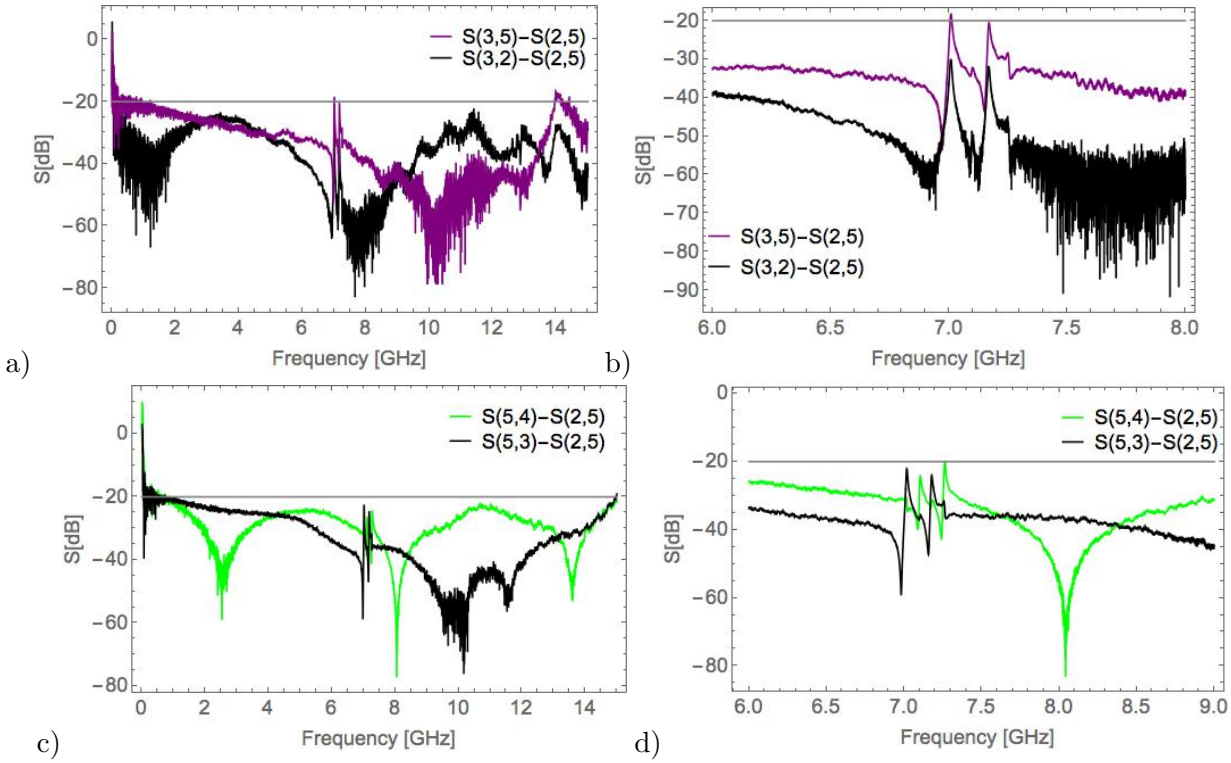


Figure 13: Difference of the crosstalk from the charge lines to the Purcell filter on M57C6 (a), b)) and on M57B2 (c), d)). Measured at 4.2 K.

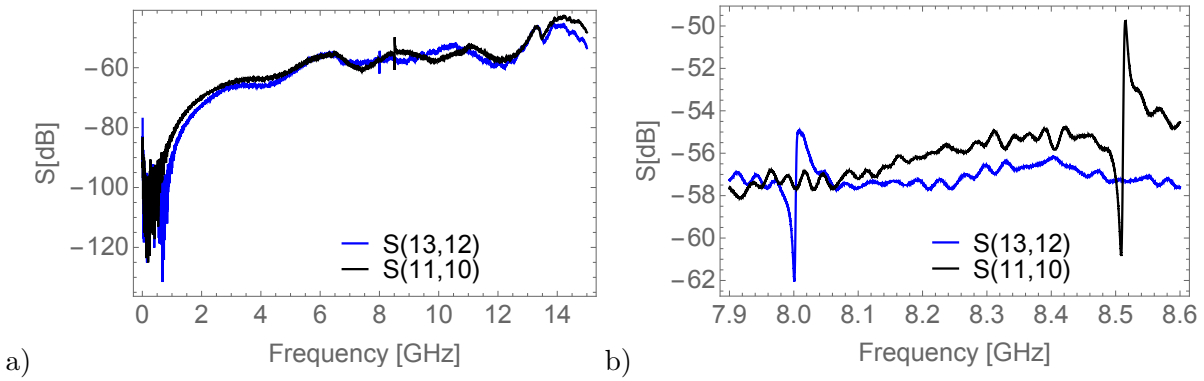


Figure 14: a) and b): Crosstalk of M57A4, are 10-11 the ports of the coupling resonator at 8.5 GHz and 12-13 the ports of the coupling resonator at 8 GHz. Measured at 4.2 K.

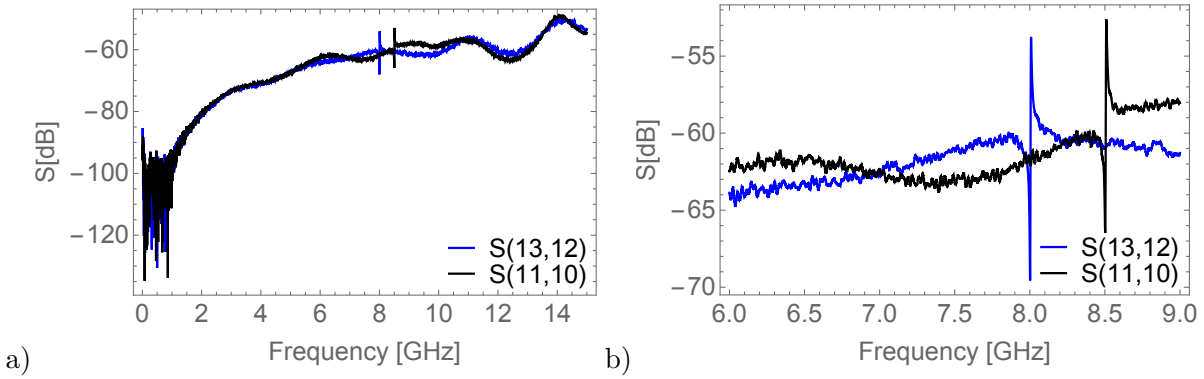


Figure 15: a) and b): Crosstalk of M57F3, 10-11 are the ports of the coupling resonator at 8.5 GHz and 12-13 the ports of the coupling resonator at 8 GHz. Measured at 4.2 K.

# 5 Conclusion

The Purcell filter and the coupling resonators were successfully characterized. The resonance frequency and the quality factor were compared with simulations using a dielectric constant $\epsilon_{eff}^{(1)} = 5.67$ (from earlier measurements) and $\epsilon_{eff}^{(2)} = 5.81$ (from a measurement in the dilution cryostat). The simulations with $\epsilon_{eff}^{(2)}$ delivered the better predictions for the resonance frequencies. This is also the case for both Purcell filters coupled to the readout resonators. For this systems the chip M57B2 has the best configuration of resonance frequencies of mask M57 since here the readout resonance frequencies are the closest to the resonance frequency of the Purcell filter. This can be improved further by lowering this resonance frequency. Combining the measured and simulated data we determined the insertion loss $L_0$ to be at around 60 dB (under-coupled Purcell filter), 0.16 dB (normally coupled Purcell filter) and 30 dB (coupling resonators).

For the under-coupled Purcell filters we measured a quality factor $Q$ of order $10^3$ and for the coupling resonators about 1450 at 4.2 K and of order $10^5$ (for both types of resonators) at 20 mK. In the latter measurements we also swept the input power and looked how $Q$ changed. This data was used to plot $Q$ vs. the estimated number of photos in the resonator. We observed that $Q$ is decreased by lowering the number of photons. For photon numbers below 20 $Q$ seems to converge and it is still in the order of $10^5$.

The crosstalk difference to the wanted transmission through the Purcell filter is below -20 dB. The higher crosstalk was between the output and the charge lines, especially in the range of the resonance frequencies of the readout resonators. To minimize this coupling the gap between the charge lines and the readout resonators should be enlarged. A crosstalk of less than -30 dB in the range without resonances is fine, since one normally does not measure and drive the qubit at the same time.

# 6 Acknowledgement

I would like to thank Prof. Dr. Andreas Wallraff for giving me the opportunity to write my semester thesis in the quantum device lab. I also thank my supervisor Yves Salathé that I could collaborate on his project and for his help.

## References


[1] M. Göppl, A. Fragner, M. Baur, R. Bianchetti, S. Filipp, J. M. Fink, P. J. Leek, G. Puebla, L. Steffen, and A. Wallraff, J. Appl. Phys. **104**, 113904 (2008)

[2] E. Jeffrey et al., Phys. Rev. Lett. **112**, 190504 (2014)

[3] P. J. Petersan and S. M. Anlage, J. Appl. Phys. **84**, 3392 (1998)

[4] Patrik Caspar, Semester Thesis (2015)

[5] D. F. Walls and G. J. Milburn, *Quantum Optics* (Springer Verlag 2008) pp. 131ff.

[6] P. Yin and X. Fan, J. Exp. Educ. **69:2**, 203-224 (2001)

[7] M. S. Khalil, M. J. A. Stoutimore, F. C. Wellstood and K. D. Osborn, J. Appl. Phys. **111**, 054510 (2012)

[8] M. Baur, Ph.D. thesis, ETH Zürich number 20359 (2012)

[9] A. Blais et al., Phys. Rev. A **69**, 062320 (2004)

[10] J. Koch et al., Phys. Rev. A **76**, 042319 (2007)

[11] E. A. Sete et al., Phys. Rev. A **92**, 012325 (2015)

ETH

Eidgenössische Technische Hochschule Zürich
Swiss Federal Institute of Technology Zurich

## Declaration of originality

The signed declaration of originality is a component of every semester paper, Bachelor's thesis, Master's thesis and any other degree paper undertaken during the course of studies, including the respective electronic versions.

Lecturers may also require a declaration of originality for other written papers compiled for their courses.

---

I hereby confirm that I am the sole author of the written work here enclosed and that I have compiled it in my own words. Parts excepted are corrections of form and content by the supervisor.

**Title of work** (in block letters):

Charakterizing the Microwave Properties of Multi-Qubit cQED Devices with Purcell Filter for Multiplexed Readout

**Authored by** (in block letters):

*For papers written by groups the names of all authors are required.*

| **Name(s):** | **First name(s):** |
|---|---|
| Heugel | Toni Louis |
| | |
| | |
| | |
| | |

With my signature I confirm that

- I have committed none of the forms of plagiarism described in the 'Citation etiquette' information sheet.
- I have documented all methods, data and processes truthfully.
- I have not manipulated any data.
- I have mentioned all persons who were significant facilitators of the work.

I am aware that the work may be screened electronically for plagiarism.

| **Place, date** | **Signature(s)** |
|---|---|
| Zurich, 22.06.2016 | Toni L. Heugel |
| | |
| | |
| | |
| | |

*For papers written by groups the names of all authors are required. Their signatures collectively guarantee the entire content of the written paper.*